Design and Economics of a Pumping KiteWind Park

Faggiani, Pietro; Schmehl, Roland

DOI
10.1007/978-981-10-1947-0_16

Publication date
2018

Document Version
Final published version

Published in
Airborne Wind Energy

Citation (APA)
Faggiani, P., & Schmehl, R. (2018). Design and Economics of a Pumping KiteWind Park. In R. Schmehl (Ed.), *Airborne Wind Energy: Advances in Technology Development* (pp. 391-412). (Green Energy and Technology; No. 9789811019463). Springer. https://doi.org/10.1007/978-981-10-1947-0_16

Chapter 16
Design and Economics of a Pumping Kite Wind Park

Pietro Faggiani and Roland Schmehl

Abstract The development of airborne wind energy is steadily progressing towards the market introduction of the technology. Even though the physical foundations of the various conversion concepts are well understood, the actual economic potential of distributed small-scale and centralized large-scale power generation under real-world conditions is still under investigation. In the present chapter we consider the clustering of units into a large kite wind park, specifically the spatial arrangement and collective operation. The analysis starts from a quasi-steady flight model of the kite to estimate the power production in pumping cycle operation. From the surface area and aerodynamic properties of the kite all other system parameters are determined. A genetic algorithm is used to optimize the operation of a single unit and to derive its power curve. Based on this information multiple interconnected units are simulated and an economic model is added. The results show that a coordinated collective operation not only achieves a continuous net electricity output, but also decreases the LCOE from 106 to 96 €/Mwh as consequence of economic scale effects. The prediction supports the substantial economic potential of pumping kite wind parks for large-scale power generation.

16.1 Introduction

A common feature of airborne wind energy (AWE) is the use of tethered flying devices for harvesting the kinetic energy of wind. Replacing the foundation and rigid tower of conventional wind turbines by lightweight tethers and control technology, AWE systems can potentially achieve lower energy costs and access wind at higher altitudes. However, apart from this common feature, the technical details and de-

Pietro Faggiani (✉) · Roland Schmehl
Delft University of Technology, Faculty of Aerospace Engineering, Kluyverweg 1, 2629 HS Delft, The Netherlands
e-mail: p.faggiani@kitepower.nl

R. Schmehl (ed.), *Airborne Wind Energy*, Green Energy and Technology, https://doi.org/10.1007/978-981-10-1947-0_16

signs of the currently pursued conversion concepts can be quite different [5]. In view of the current development activities, the pumping kite power system (PKPS) with either flexible or rigid wings seems to be a clear industry favorite because of its conceptual simplicity and scalability.

The presented study is based on the PKPS concept. The considered implementation is using a leading edge inflatable (LEI) tube kite operated on a single tether and steered by a remote-controlled suspended kite control unit (KCU), as illustrated in Fig. 16.1 and described in more detail in [25]. To maximize the tether tension

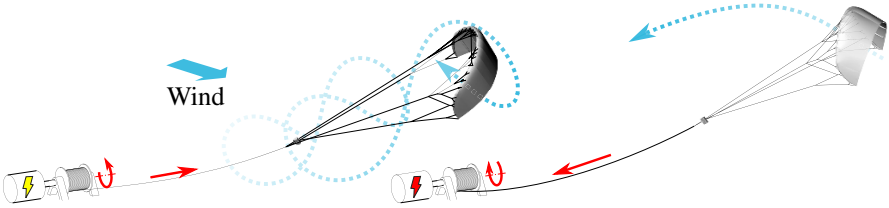

Fig. 16.1 Schematic representation of the pumping cycle: traction phase with crosswind flight maneuvers (left) and retraction phase with de-powered wing (right). Adapted from [25]

during the traction phase the kite is steered in crosswind flight maneuvers while the tether is being reeled from a drum. This rotational motion drives the connected generator. Reaching a predefined altitude, the kite is de-powered to minimize the tether tension. The tether is then reeled back onto the drum consuming a fraction of the energy produced in the previous phase. When reaching the minimum tether length the next traction phase is started. Energy is thus generated in pumping cycles. Because the flight motion of a lightweight tethered wing is dominated by the equilibrium of aerodynamic, tether and gravitational forces a quasi-steady theoretical model can be used to efficiently predict the mechanical power production or consumption of the kite at different wind speeds and in different operational phases [7, 22, 24]. Extending this framework to all components of the kite power system, the global energy conversion efficiency is broken down to the efficiencies of the individual system components [12].

The objective of the present study is to analyze the economic potential of the pumping kite power technology under real-world conditions, considering a wind park configuration. Specific elements of such analysis have already been treated, for example, the economics of single systems [2, 15, 17] or the spacial arrangement in a wind park [14]. However, only few recent studies have quantitatively compared the characteristics of conventional wind turbines and AWE systems and extended this to large-scale park configurations [6, 8]. Starting point of the present analysis is the approach described in [17], which governs the economics of a single PKPS and which we develop into a framework to assess a kite wind park in terms of the achievable levelized cost of energy (*LCOE*). This measure quantifies the cost per unit of produced energy in €/MWh throughout the project lifetime, allowing a consistent comparison with other energy technologies. The *LCOE* is evaluated as

the ratio of the discounted costs C_t of the installation, accumulated over the years $t = 1,\ldots,n$ of its lifetime, and the discounted energy E_t produced, equally accumulated over the years

$$LCOE = \frac{Cost}{Energy} = \frac{\sum_{t=1}^{n} \frac{C_\mathrm{t}}{(1+i)^t}}{\sum_{t=1}^{n} \frac{E_\mathrm{t}}{(1+i)^t}}, \tag{16.1}$$

where the parameter i denotes the discount rate. Costs can be divided into operational and maintenance costs OMC, expressed in €/y, and initial capital costs ICC, expressed in €. If the annual energy production AEP, expressed in MWh/y, is constant we can write

$$LCOE = \frac{ICC \times CRF + OMC}{AEP}, \tag{16.2}$$

using the capital recovery factor CRF, which takes into account the time value of money. This parameter can be computed for the lifetime of the system as

$$CRF = \frac{i(1+i)^n}{(1+i)^n - 1}. \tag{16.3}$$

Evaluating Eq. (16.1) requires detailed knowledge of the system performance at the specific deployment location and of the associated cost components. Because all commercial development programs are still in a prototype stage, the scale effects of mass production are taken into account by reasonably estimated cost reductions.

The chapter is organized as follows. In Sect. 16.2 a quasi-steady flight model of the kite is developed to derive the power curve of a single PKPS. The approach is based on [22, 24] but several aspects of the analytical framework have been simplified to reduce the computational effort without considerably affecting the result quality. In Sect. 16.3 a genetic algorithm is used to optimize the main operational parameters of the system for maximizing the energy production at every wind speed. In Sect. 16.4 multiple PKPS are used in a wind park configuration, investigating the effects of the spacial arrangement, the modes of operation depending on the wind direction, the control strategy and the electrical interconnection of the units. In Sect. 16.5 a basic cost model is used to determine the LCOE of the wind park configuration. The influence of the initial parameter choices and assumption is investigated by a sensitivity analysis. The preliminary content of the present chapter has been presented at the Airborne Wind Energy Conference 2015 [11] and is described in detail in [10].

16.2 Quasi-Steady Flight Model

The flight motion of a kite operated in pumping cycles can be described, for most of the time, as a quasi-steady transitioning through equilibrium states. This obser-

vation can be used to formulate an efficient model to predict the traction power and energy production over a pumping cycle as function of the system design and operational parameters. To account for the different kinematics and force balances in the retraction, transition and traction phases the cycle is generally discretized along the flight trajectory.

16.2.1 Theoretical Framework

The present study is based on the quasi-steady flight model developed in [22] and further detailed, extended to pumping cycle operation and validated experimentally in [21, 24]. Starting point is the Cartesian wind reference frame x_w, y_w, z_w, which is centered at the tether ground attachment point **O**, has its x_w-axis oriented along the wind velocity vector $\mathbf{v}_w$ and is assumed to be an inertial frame. The kite position **K** is described in spherical coordinates (r, θ, ϕ) as illustrated in Fig. 16.2. Assuming that

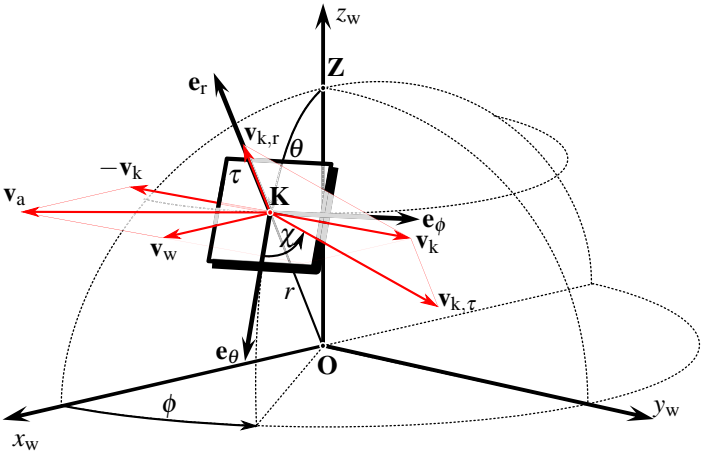

Fig. 16.2 Definition of the apparent wind velocity $\mathbf{v}_a = \mathbf{v}_w - \mathbf{v}_k$. Decomposition of the kite velocity $\mathbf{v}_k$ into radial and tangential components $\mathbf{v}_{k,r}$ and $\mathbf{v}_{k,\tau}$, respectively. The course angle χ is measured in the tangential plane τ, the spherical coordinates (r, θ, ϕ) are defined with respect to the wind reference frame x_w, y_w, z_w. The tether elevation angle is defined as $\beta = 90° - \theta$. Figure and caption from [22]

the tether is straight, the flight motion can then be decomposed into a radial velocity component $\mathbf{v}_{k,r}$, which is controlled by the ground station, and a tangential velocity component $\mathbf{v}_{k,\tau}$. The course angle χ describes the direction of $\mathbf{v}_{k,\tau}$ with respect to the local unit vector $\mathbf{e}_\theta$ and it is controlled by the steering system of the kite. However, the magnitude $v_{k,\tau}$ of the tangential velocity component is a dependent problem variable and not a kinematic degree of freedom [22]. The corresponding non-dimensional velocity components are denoted as reeling factor f and tangential

velocity factor λ defined as

$$f = \frac{v_{\mathrm{k,r}}}{v_{\mathrm{w}}} \qquad \text{and} \qquad \lambda = \frac{v_{\mathrm{k},\tau}}{v_{\mathrm{w}}}. \tag{16.4}$$

The mass of the kite, its control unit and part of the tether are taken into account as a lumped mass located at point **K**. Similarly the resultant aerodynamic force generated by the kite and part of the aerodynamic drag acting on the tether are lumped to point **K**. The quasi-steady flight behavior is governed by the equilibrium of the resultant aerodynamic force, gravitational force and tether force. Each pumping cycle is divided into a sequence of traction, retraction and transition phases and the aerodynamic properties of the kite are assumed to be constant for each phase.

To account for the varying kinematics and forces the flight path $\mathbf{r}_{\mathrm{k}}$ is advanced in discrete time steps Δt according to the finite difference scheme

$$\mathbf{r}_{\mathrm{k}}(t+\Delta t) = \mathbf{r}_{\mathrm{k}}(t) + \mathbf{v}_{\mathrm{k}}(t)\Delta t. \tag{16.5}$$

The control strategy for the simulation is based on set values for the tether force F_{t} which are achieved by adjusting the reeling factor according to [22]

$$f = \sin\theta\cos\phi - \sqrt{\frac{F_{\mathrm{t}}}{qS_{\mathrm{k}}C_{\mathrm{R}}\left(1+\kappa^2\right)}}, \tag{16.6}$$

where q denotes the dynamic wind pressure

$$q = \frac{1}{2}\rho v_{\mathrm{w}}^2, \tag{16.7}$$

the resultant aerodynamic coefficient is evaluated as

$$C_{\mathrm{R}} = \sqrt{C_{\mathrm{L}}^2 + C_{\mathrm{D}}^2}, \tag{16.8}$$

the kinematic ratio is given by

$$\kappa = \frac{v_{\mathrm{a},\tau}}{v_{\mathrm{a,r}}}, \tag{16.9}$$

and S_{k} denotes the projected area of the kite. For vanishing mass of the airborne components, κ is identical to the lift-to-drag ratio $C_{\mathrm{L}}/C_{\mathrm{D}}$. For real systems this idealization does not hold anymore and Eq. (16.6) has to be solved iteratively [22, 24].

16.2.2 Retraction Phase

The simulation of the pumping cycle starts with the retraction phase because it is only at the start of this phase that the kite position is fully defined by the model

settings. The kite is fully de-powered to its minimum lift-to-drag ratio C_L/C_D to consume as little energy as possible for the retraction flight maneuver. Adjusting the course angle to $\chi = 180°$ the kite flies against the wind, with azimuth angle $\phi = 0°$, while the tether elevation angle β continuously increases. The tether length is at its maximum at the start of this phase and at its minimum when the end is reached.

For low reel-in velocity $v_{k,r}$ the kite can reach a steady flight state on a radial trajectory descending towards the ground station. For higher reel-in velocity, as generally used in practice, this steady-state flight condition with $\lambda = 0$ and constant β_{max} is approached asymptotically but not reached before switching to the transition phase. This is clearly visible in Fig. 16.3 which shows a representative computed trajectory. Because of the high reel-in velocity in this particular case the kite overflies the ground station in upwind direction to positions $x < 0$.

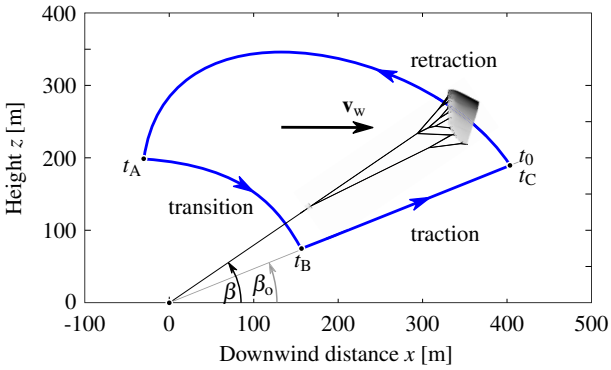

Fig. 16.3 Two-dimensional flight trajectory computed with the quasi-steady model. The radial line segment $\beta_o = \text{const.}$ representing the traction phase does not resolve the crosswind flight maneuvers but is computed on the basis of an averaged flight state. The time integration starts at t_0, the transition phase at t_A, the traction phase at t_B and the cycle ends at t_C

16.2.3 Transition Phase

At the end of the retraction phase the elevation angle is much larger than the design value for the traction phase. The purpose of the transition phase is to perform a flight maneuver that brings the kite back to the elevation angle that governs the traction phase. For this maneuver the kite is again fully powered such that it has the aerodynamic properties of the traction phase. The kite flies in downwind direction with course angle $\chi = 0$ until it reaches the target elevation angle for the traction phase.

The control strategy during this phase is not based on the tether force but on the reeling velocity. The aim is here to fly the maneuver at constant tether length, which means that Eq. (16.6) needs to be solved for F_t, setting $f = 0$. However, any implemented AWE system will need to maintain a certain minimum tension in the tether to ensure operational stability. For the present simulation, the minimum

tension limit is applied to the entire pumping cycle by means of adjusting the reeling velocity. For example, when the tension drops below the limiting the tether is reeled in such that the tension increases again.

16.2.4 Traction Phase

In the traction phase the kite is flown in crosswind maneuvers to maximize the apparent wind velocity at the wing and correspondingly also the traction force. Because circular flight maneuvers can lead to torsion of the tether and entanglement of the bridle line system it is common to use flight maneuvers that track a horizontal figure of eight. To maximize the traction power the maneuvers are generally centered at $\phi = 0$, as illustrated in Fig. 16.4.

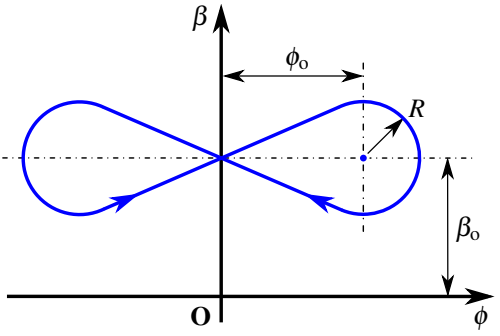

Fig. 16.4 Representative figure of eight flight maneuver in the $\phi\beta$-plane [13]. In Cartesian space this plane represents a spherical surface around the origin

Instead of resolving the actual physical flight path of a crosswind maneuver, the present approach uses a constant average flight state to compute the generated traction force. Accordingly, the varying tangential motion in the $\phi\beta$-space is represented by a constant average angular position (ϕ_o, β_o) and flight velocity (λ_o, χ_o). This approach substantially reduces the computational effort because the crosswind maneuver can be optimized separately and the flight path can be integrated in two dimensions, as illustrated in Fig. 16.3. The values ϕ_o, β_o and χ_o are determined as time averages of the real flight state over a crosswind maneuver. Because the traction power is a function of the product term $\cos\phi\cos\beta$ we define the positional averages by

$$\cos\phi_o = \overline{\cos\phi} \qquad \text{and} \qquad \cos\beta_o = \overline{\cos\beta}. \tag{16.10}$$

These definitions result in an average angular position (ϕ_o, β_o) coinciding with the center of the lobe of the figure of eight, as illustrated in Fig. 16.4. Because of gravity the kite is flying slower in upward than in downward direction the average course angle χ_o is larger than 90°, which is the value characterizing horizontal flight. The traction phase is completed when the tether reaches its maximum length at t_C. The position of the kite at this time coincides with its initial position at t_0.

16.2.5 Complete Cycle

With the averaging of the crosswind flight trajectory in the traction phase the pumping cycle can be analyzed in a two-dimensional framework. The side view of a representative computed trajectory is illustrated in Fig. 16.3. The mean mechanical net power is computed as time average of the power provided or required by the system over one cycle

$$P_\mathrm{m} = \frac{\overline{P}_\mathrm{o}\Delta t_\mathrm{o} + \overline{P}_\mathrm{x}\Delta t_\mathrm{x} + \overline{P}_\mathrm{i}\Delta t_\mathrm{i}}{\Delta t_\mathrm{o} + \Delta t_\mathrm{x} + \Delta t_\mathrm{i}}, \tag{16.11}$$

where the subscripts refer to traction (o), transition (x) and retraction phases (i). Equation (16.11) is maximized by an optimization procedure that is discussed in the following section.

16.3 Optimization

The present analysis considers the size of the kite to be a prescribed design parameter which is not varied during the optimization process. All other design parameters are scaled accordingly following system-level engineering practices to minimize losses, while meeting the specific technical requirements and complying with physical and regulatory limitations. Once the design parameters are set, the operational parameters of the system are determined by systematic optimization. In its outermost loop the computational framework steps through the range of expected wind speeds in discrete increments to determine the power curve of the system.

16.3.1 Methodology

To maximize the power production of any wind energy system it is crucial to adjust the operational parameters to the available wind resource. Analyzing the potential of kites for power generation, Loyd [18] found that the tether of a kite flying in crosswind direction should be reeled out with $1/3$ of the wind speed to maximize the produced power. Although this idealized theory neglects the effect of gravity on kite and tether as well as the effect of aerodynamic drag on the tether it provides a fundamental understanding of the mechanism of traction power generation and thus represents a first basic guideline for optimization.

More accurate models have been developed subsequently to describe the influence of a broader set of problem parameters and also of gravitational and inertial force contributions that can significantly affect the operation of the kite [1, 19, 22]. However, with increasing mathematical complexity an explicit analytical solution is not possible anymore and as consequence numerical solution techniques are re-

quired. The work of Grete [15] is used as reference to choose the most important operational parameters to be optimized. Those are the tether forces during traction and retraction phases, $F_{t,o}$ and $F_{t,i}$, the minimum and maximum tether lengths, $l_{t,min}$ and $l_{t,max}$ as well as the average elevation angle in the traction phase, β_o.

The tether reeling speed is continuously adjusted by the winch control system to meet the constant set values of the tether force for each cycle phase. This radial velocity has a dominating influence on the instantaneous traction power and the system reacts very sensitively to deviations from its optimal value. The optimization of the minimum and maximum tether length is motivated by the observation that the wind power density generally increases with flight altitude while the aerodynamic drag and gravitational forces acting on the tether increase with the deployed length. The competing effect on the traction power leads to an altitude range which maximizes the power production of the kite power system. The sensitivity of the power output to the average elevation angle in the traction phase is rather low. While the power output does not change notably within a range of $\pm$ 5° it does decrease rapidly for values far away from the optimum value.

Because the power output of the pumping cycle is the result of a numerical integration which depends on several operational parameters that are optimization variables, a Monte Carlo genetic algorithm is used. The approach starts from parameter sets that are chosen randomly within specified ranges. In genetic algorithm terminology these sets represent families which together form a generation of the population. Among the families only those performing best in terms of power production are retained for the next generation of the population. An effort is made to restrict the parameter ranges to practically suitable limits in order to reduce the computational effort. To achieve this the ranges are derived from the optimization results obtained for the previous wind speed.

It is important to note that the traction power is subject to several physical constraints. The maximum wing loading and the maximum tether loading both impose a limit on the tether force that can be reached. Additional limiting factors are the reeling speed and the nominal power of the electrical machines on the ground. When neither the tether force nor the reeling speed can be increased anymore to compensate for a large wind speed the kite has to be depowered.

16.3.2 Case study

In this section we present a case study to demonstrate the performance of the modelling and optimization framework. Considering a utility-scale energy system we chose a wing surface area of 100 m^2 for the kite. The derived design parameters of the system as well as the aerodynamic properties of the kite are summarized in Table 16.1. For each discrete wind speed in the considered range, the operational parameters are optimized for maximum power. The result is the power curve of the pumping kite power system. The computation of the curve shown in Fig. 16.5 has taken about 30 minutes on a standard Laptop.

Table 16.1 Design parameters and aerodynamic parameters of a representative pumping kite power system for utility-scale energy generation

Parameter name	Symbol	Value	Unit
Total wing surface area	A_k	100	m^2
Projected wing surface area	S_k	72	m^2
Kite mass	M_k	48	kg
Kite control unit mass	M_{kcu}	16	kg
Maximum wing loading		450	N/m^2
Tether diameter	d_t	12	mm
Aerodynamic lift coefficient	C_L		
• retraction phase		0.3	
• transition & traction phases		0.8	
Aerodynamic drag coefficient	C_D		
• retraction phase		0.1	
• transition & traction phases		0.2	

With increasing wind speed the power output reaches a maximum value and then continuously decreases. This behavior at larger wind speeds is not known from conventional wind turbines. It can be explained by the fact that above a certain wind speed the energy required for the retraction keeps increasing, while the energy produced in the traction phase remains constant or decreases due to physical limitations, such as the maximum tether force, for example.

Together with a the probability distribution of the wind speed at the specific location the annual energy production (AEP) of the system can be determined.

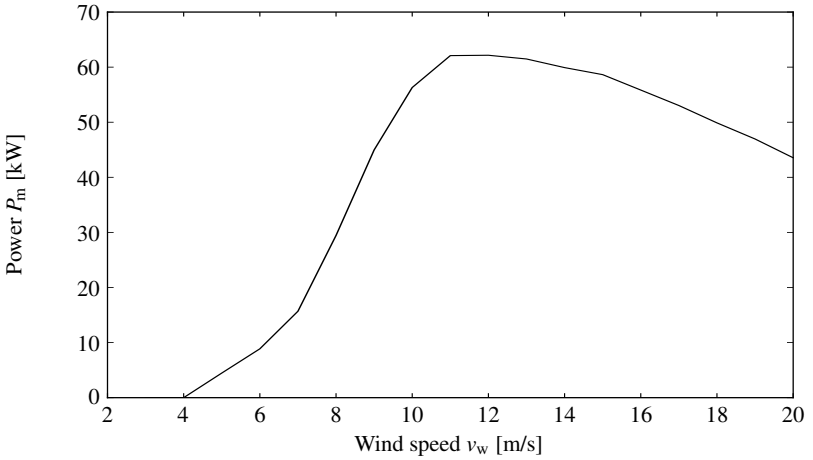

Fig. 16.5 Power curve of a pumping kite power system equipped with a 100 m^2 kite having aerodynamic properties as listed in Table 16.1

16.4 Wind Park Arrangement

The optimized unit is used as building block for a complete kite wind park. In the following sections we investigate how pumping cycle characteristics affect the collective operation in a park configuration. Specific aspects are the spacial arrangement of the units, the quantity and quality of the generated electricity as well as the economic performance.

16.4.1 Spacing of Units

For conventional wind parks the aerodynamic interaction between turbines strongly depends on the inter-turbine spacing because the energy is harvested from the atmospheric layer close to the ground surface. In contrast to that, a crosswind kite operated in pumping cycles covers a substantially larger airspace and as consequence wake interaction effects are assumed to be negligible. This can be justified by the relatively small wing surface area compared to the swept area of the kite. Moreover, the kites can be flown at different heights and maneuvered in such a way as to avoid perfect alignment with the wind.

In the present study the spacing between units is determined by the requirement of safe collective operation. This requirement has already been applied in previous work on the subject [14, 17]. The flight envelope of each unit is designed in such a way that mechanical interference between the airborne components is avoided. The most restrictive distance constraint is required for units that are aligned with the wind direction, such as illustrated in Fig. 16.6. In this sketch the maximum tether length resulting from the optimization process is denoted as L, the maximum radius of the operational envelope as R, the opening angle of the operational envelope as ν and the distance between two units as d_u.

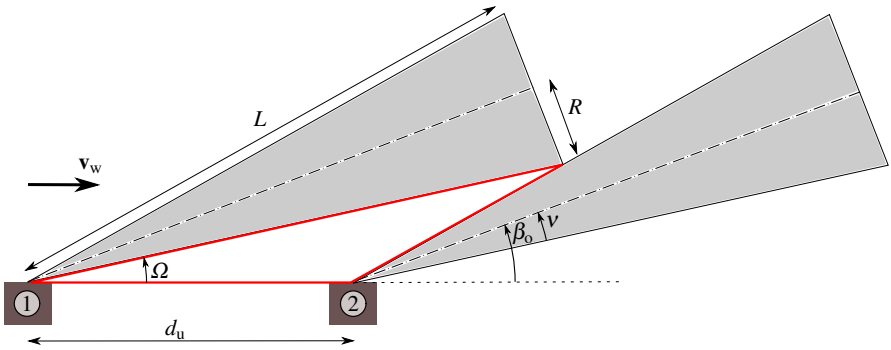

Fig. 16.6 Side view of two units aligned with the wind direction, with the shaded areas defining the operational envelopes

We follow the approach described in [16] to determine the minimum safe distance to avoid collision of airborne components. Starting point is the red triangle highlighted in Fig. 16.6 which can be used to formulate the expression [11]

$$d_\mathrm{u} = \frac{L}{\sin(\beta_\mathrm{o} - \nu_1)\left[\frac{1}{\tan(\beta_\mathrm{o}-\nu_1)} + \frac{1}{\tan(\nu_1+\nu_2)}\right]}, \tag{16.12}$$

where indices 1 and 2 refer to the upwind and downwind units, respectively. To minimize Eq. (16.12) the two units have to be operated synchronously, which, for cyclic pumping operation means that they have to be operated in phase. Although smaller deviations from synchronous operation can be covered by application of a safety factor, a robust supervisory control strategy has to be implemented to prohibit larger phase differences. This is of particular importance when the units are aligned with the wind direction.

However, while synchronous operation allows a close spacing of the units it is not favorable from the power production perspective. We will show in the following section that collective operation with different phase shifts has an equalizing effect on the output power which improves the quality of the electricity delivered to the network.

To estimate the maximum radius R of the operational envelope we assume that the kite is operated in figure eight maneuvers, as illustrated in Fig. 16.4. Starting point is the turn rate law [9]

$$\dot{\chi} = g_\mathrm{k} v_\mathrm{a} \delta, \tag{16.13}$$

which is a mechanistic model describing how the non-dimensional steering input δ and the apparent wind velocity v_a influence the time derivative of the course angle χ. In this equation the maneuverability g_k is regarded as an empirical constant that can be determined experimentally or by high-resolution computational simulation of the flexible ad deforming kite [4]. The turn rate is coupled to the radius R and the tangential flight velocity $v_{\mathrm{k},\tau}$ by the kinematic relation (see Fig. 15.9 in this book)

$$v_{\mathrm{k},\tau} = R\dot{\chi}, \tag{16.14}$$

noting that for crosswind maneuvering $v_{\mathrm{k},\tau}$ can be calculated as shown in [22]. Knowing the maximum radius of the circular trajectory segments and the maximum tether length we can determine the opening angle from

$$\nu = \arcsin\frac{R}{L} \tag{16.15}$$

and the minimal distance from Eq. (16.12).

For the considered kite size of 100 m^2 we calculate a turning radius of approximately 50 m, which results in a minimal distance of 100 to 150 m between units. Figure 16.7 shows the result of a parametric analysis, investigating the influences of the elevation angle and the maximum radius of the operational envelope.

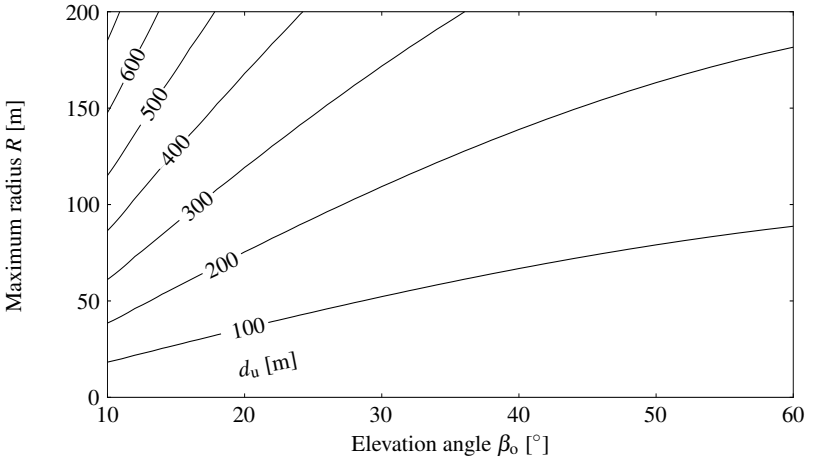

Fig. 16.7 Isolines of the minimum distance d_u between two units as function of the elevation angle β_o during traction and the maximum radius R of the operational envelope. In this specific case a maximum tether length of $L = 1500$ m has been assumed

16.4.2 Quality of Electricity Output

For simplicity we consider a square array layout of the farm. Neither the temporal variability of the wind direction nor the flow interaction between kites is taken into account at this stage. The wind direction is used as a reference to define columns and rows of kite power systems. The units roughly aligned with the wind direction are grouped into columns, while the units roughly aligned in perpendicular direction are grouped into rows. The two extreme inflow scenarios are depicted in Fig. 16.8

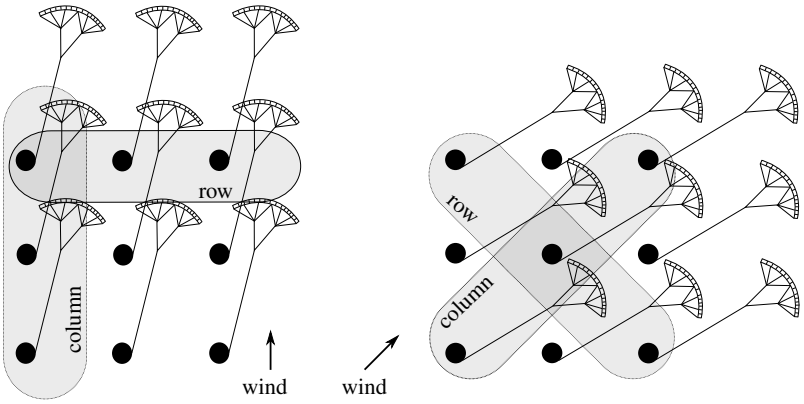

Fig. 16.8 Inflow aligned with array layout of wind farm (left) and diagonal to array layout (right)

indicating that diagonal inflow leads to a maximum asymmetry of the distribution of units into columns and rows.

In the previous section we have shown that units in columns need to be operated synchronously, without significant phase shift, to allow a close spacing. Across the columns, on the other hand, units can be operated safely with phase shifts to internally balance the electricity output of the farm. From these considerations it is clear that the inflow direction plays an important role, affecting the collective operation and production characteristics of the wind farm. In the following we detail the operational strategy on farm level.

For inflow aligned with the array, the phase shift between the columns is calculated as the cycle period divided by the number of columns. For diagonal inflow, the phase shift is calculated as twice this value, which ensures that the outer columns with fewer units are synchronized and in opposite phase to the inner columns with more units. To account for imperfect control a small phase shift is applied between units in the same column. The minimal distance is determined as a function of the maneuverability of the kite and the maximum phase shift of the units in the same column.

The key parameters influencing the power output of a wind farm are the number of units as well as the direction and the magnitude of the wind speed. The instantaneous power output of a single pumping kite power system and two farm configurations of different sizes is illustrated in Fig. 16.9. The simulations show that with the

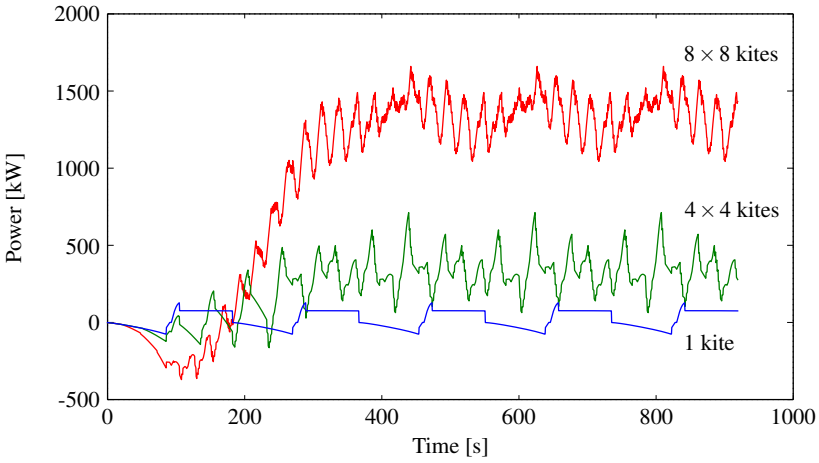

Fig. 16.9 Instantaneous electricity generation of kite wind farms with a wing surface area of 100 m^2 per kite. Inflow diagonal to the array with a wind velocity of 8 m/s

number of contributing units the fluctuation frequency as well as the average output power increase. We further conclude that the farm configuration with the largest number of units can be operated over the broadest wind speed range [10]. Because

of the internal load balancing of the units the need for temporary energy storage to retract the kites can be substantially reduced for larger farms.

The generated traction power and the consumed retraction power of the individual units increase strongly with the wind speed and as a result also the fluctuation amplitude of the instantaneous power output of the farm increases. To quantify the quality of the electricity output we use the normalized standard deviation. The simulation results show that by introducing phase shifts, as discussed above, the deviation can be reduced to the minimum for all combinations of wind speed and direction.

Figure 16.10 shows the result of a parametric analysis for array-aligned and diagonal inflow. The standard deviation decreases with increasing wind speed as long as the average cycle power increases. The latter is evident from the power curve of the single unit, illustrated in Fig. 16.5, which peaks at a wind speed of 12 m/s. Above this value the average cycle power decreases because the retraction power further increases while the traction power is limited by the maximum loading constraint. As consequence the standard deviation increases because it is inversely proportional to the average power.

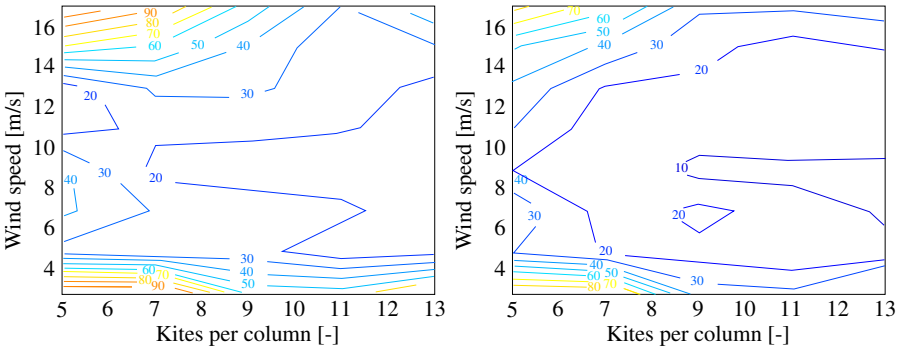

Fig. 16.10 Isolines of the normalized standard deviation for inflow aligned with the array layout of the farm (left) and diagonal to the array layout (right)

With increasing number of kites the standard deviation decreases. The effect is stronger for diagonal inflow because the non-uniform distribution of units to columns allows a better internal balancing of the power contributions.

16.5 Economic Performance

To estimate the levelized cost of energy a simple cost model is added to the simulation framework. The different cost items, their parametric dependencies and the resulting values used for this analysis are listed in Table 16.2. The costs functions are adapted from previous works on wind turbine farms [26] or from specific literature on kite power systems [15, 16]. The specific cost values refer to a wind farm

based using kites of $A_k = 100$ m^2 surface area, for which the power curve has been presented in Fig. 16.5. The rated continuous power of the individual units, after balancing internally with an energy storage system or on park level among the units, is $P_{rat} = 60$ kW. The nominal power of the electrical machines of the individual units is $P_{nom} = 100$ kW. We assume a square array layout of the farm with 7×7 individual units and a discount rate of 5% [20].

Hardware				[€/unit]
Electrical machines	C_{em}	$=$	$c_{em}\omega_{nom}^{-0.6}P_{nom}$	15000
Drum	C_{dr}	$=$	$c_{dr,1}M_{dr} + c_{dr,2}d_{dr}$	3200
Power electronics	C_{pe}	$=$	$c_{pe}P_{nom}$	2300
Transformer	C_{tr}	$=$	$(c_{tr,1}P_{rat} + c_{tr,2})e^{c_{tr,3}r_{tr}}$	4200
Tether handling and bearings	C_{thb}	$=$	$c_{thb}F_{t,max}^{0.5}$	9000
Cover frame	C_{cf}	$=$	$c_{cf,1}P_{nom}^{0.85} + c_{cf,2}$	300
Launching and landing	C_{ll}	$=$	$c_{ll}M_kA_k^{0.5}$	4800
Kite	C_k	$=$	$c_kA_k^{0.75}$	22000
Kite Control Unit	C_{kcu}	$=$	$c_{kcu,1} + c_{kcu,2}A_k^{0.5}$	3000
Tether	C_t	$=$	$c_tL\pi d_t^2/4$	9000
Electrical connections	C_{ec}	$=$	$c_{ec}d_u$	23000
Controls	C_{co}	$=$	$c_{co}P_{nom}^{0.2}$	3000
Total	C_{unit}			98800

Operation and Maintenance				[€/unit/y]
Consumables	C_{cons}			17000
O&M	C_{om}	$=$	$c_{om,1}AEP + c_{om,2}$	4000
Insurance	C_{ins}	$=$	$c_{ins}C_{unit}$	1300
Land lease	C_{land}	$=$	$c_{land}AEP$	300

Installation and Decommissioning				[€]
Transport	C_{mov}	$=$	$c_{mov}P_{nom}n_u$	196000
Civil works	C_{cw}	$=$	$c_{cw}d_un_u$	241000
Cables installation	C_{ci}	$=$	$c_{ci}{d_u}^{0.5}n_u$	6555000
Farm design	C_{fd}	$=$	$c_{fd}P_{rat}n_u$	55000
Units removal	C_{ur}	$=$	$c_{ur}Mn_u$	241000
Cables removal	C_{cr}	$=$	$c_{cr}d_un_u$	6555000

Table 16.2 Cost items taken into account by the model as functions of the total wing surface area A_k, system mass M and rated continuous power output P_{rat} per unit, component masses M_k and M_{dr}, drum diameter d_{dr}, nominal power P_{nom} and rotational speed ω_{nom} of the electrical machines, winding ratio r_{tr} of the transformer, number of units in the farm n_u, distance between the units d_u and their individual annual energy production AEP [10]. The symbols c denote constants. The values assigned are for an array of 7×7 units powered by kites of 100 m^2 surface area

Of particular interest are the scale effects on the costs. The results indicate that the step from single unit to wind farm reduces the cost of energy by 5%. Increasing the number of units, the combined effects of increasing energy production and scale effect on the installation and cable costs of the farm, reduce the investment asymptotically.

The computed LCOE of the kite wind farm is illustrated in Fig. 16.11 as function of the number of units. This prediction is in line with the cost of comparable renewable energy technologies, specifically it is in between the cost of conventional onshore and offshore wind energy. The diagram shows that for a wind farm of 49 units the cost of energy is just below 120 €/MWh.

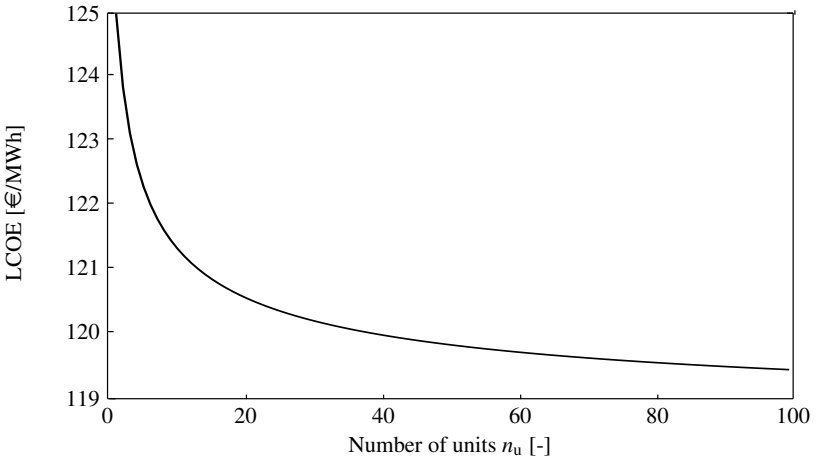

Fig. 16.11 Levelized cost of energy as function of the number of units in the farm based on 100 m^2 wing surface area per unit

The annual electricity production (AEP) of a single unit is computed as 162 MWh/y. When considering operation of the unit at the rated power of 60 kW in a wind environment that can be described by a Weibull probability distribution with parameters $k = 2$ and $A = 12$ a capacity factor of 54% can be achieved. For a wind energy system in the 100 kW range this factor is remarkably high. It is caused by the the low cut-in wind speed which enables the system to produce energy already at very low wind speeds and to access more steadier and stronger winds at higher altitudes.

The areal power density of 6 W/m^2 is comparable to the values of conventional wind turbines farms. This is a remarkable finding considering the much smaller nominal power of the kite power systems. The high power density is the result of a close spacial arrangement, assuming the availability of a suitable control strategy. However, the present analysis has not accounted for possible flow interaction effects between kites, which is left for investigation by follow-up studies.

The sensitivity analysis shows a strong influence of the wing loading and wing surface area on the LCOE. Increasing the wing loading also increases the annual energy production and therefore lowers the LCOE. The maximum wing loading is a design parameter that depends on material properties and the specific design of the kite, including its bridle system, however, these aspects are not in the scope of the present study. As illustrated in Fig. 16.12, increasing the wing size has the same effect until the higher price of larger kites outbalances the gain in terms of energy production. Given the presented cost model the optimum kite size is at around 250 m^2.

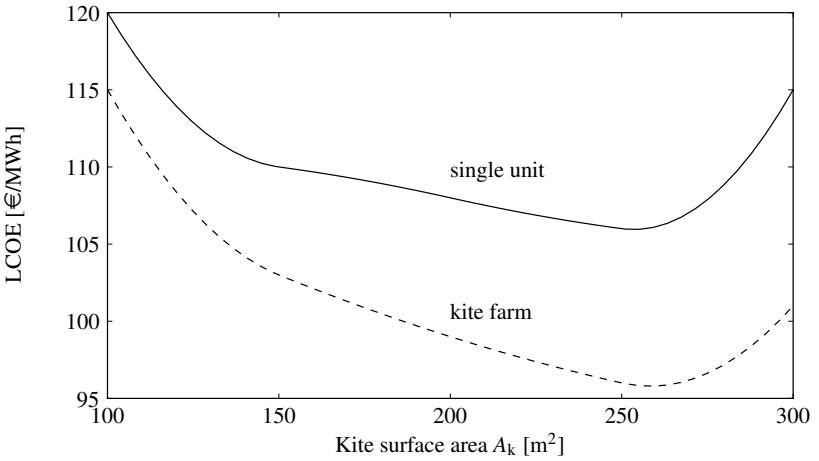

Fig. 16.12 Levelized cost of energy as function of the total wing surface are per unit

16.6 Conclusion

The presented computational approach uses the size of the kite as a starting point to dimension all other functional components of the pumping kite power system. To maximize the harvesting performance the key operational parameters are optimized for the entire range of expected wind speeds. Arranging multiple systems in a wind farm and synchronizing their operation in dependence of the wind direction it is possible to internally balance the collective power generation to create a more uniform electricity output. To assess the economic performance of the wind farm the simulation framework is complemented by a cost model that accounts for the different parametric relations of cost items.

The analysis reveals several scale effects with increasing number of kites, most notably the decreasing cost of energy and the increasing quality of the electrical

power. Considering a square array layout of the farm, a minimum cost of 96 €/MWh is achieved for units equipped with kites of 250 m^2 surface area. The corresponding cost for a single kite power power system is 105 €/MWh.

Within the scope of the study it was not possible to cover all options for further optimization. For example, we did not investigate the effect of different kite designs, such as semi-rigid or rigid wings. These are generally heavier and more expensive than flexible membrane wings, but in turn have a better aerodynamic performance, can sustain a higher wing loading and are more durable. Not surprisingly, the analysis showed that the wing loading is the most limiting property of the currently analyzed kite power system. Another component with a considerable optimization potential is the tether. The aerodynamic line drag substantially affects the power production and together with the gravitational effect limits the optimal operating altitude.

The offshore deployment of kite wind parks is a particularly interesting solution for large-scale energy generation. The pumping kite power systems are suitable for mounting on floating platforms because of the low mass and negligible bending moment occurring at the ground station. The application is explored further in Chap. 7 of this book and pursued in current industry projects [3, 23].

Acknowledgements The financial support of the European Commission through the projects AWESCO (H2020-ITN-642682) and REACH (H2020-FTIPilot-691173) is gratefully acknowledged.

References

1. Argatov, I., Rautakorpi, P., Silvennoinen, R.: Estimation of the mechanical energy output of the kite wind generator. Renewable Energy **34**(6), 1525–1532 (2009). doi: 10.1016/j.renene.2008.11.001
2. Argatov, I., Shafranov, V.: Economic assessment of small-scale kite wind generators. Renewable Energy **89**, 125–134 (2016). doi: 10.1016/j.renene.2015.12.020
3. Bloomberg New Energy Finance: Shell will test energy-generating kites this summer. BNEF Blog, 26 May 2017. https://about.bnef.com/blog/shell-will-test-energy-generating-kites-this-summer/ Accessed 30 May 2017
4. Bosch, A., Schmehl, R., Tiso, P., Rixen, D.: Dynamic nonlinear aeroelastic model of a kite for power generation. AIAA Journal of Guidance, Control and Dynamics **37**(5), 1426–1436 (2014). doi: 10.2514/1.G000545
5. Cherubini, A., Papini, A., Vertechy, R., Fontana, M.: Airborne Wind Energy Systems: A review of the technologies. Renewable and Sustainable Energy Reviews **51**, 1461–1476 (2015). doi: 10.1016/j.rser.2015.07.053
6. Coleman, J., Ahmad, H., Pican, E., Toal, D.: Modelling of a synchronous offshore pumping mode airborne wind energy farm. Energy **71**, 569–578 (2014). doi: 10.1016/j.energy.2014.04.110
7. Costello, S., Costello, C., François, G., Bonvin, D.: Analysis of the maximum efficiency of kite-power systems. Journal of Renewable and Sustainable Energy **7**(5), 053108 (2015). doi: 10.1063/1.4931111

8. De Lellis, M., Mendonça, A. K., Saraiva, R., Trofino, A., Lezana, Á.: Electric power generation in wind farms with pumping kites: An economical analysis. Renewable Energy **86**, 163–172 (2016). doi: 10.1016/j.renene.2015.08.002
9. Erhard, M., Strauch, H.: Theory and Experimental Validation of a Simple Comprehensible Model of Tethered Kite Dynamics Used for Controller Design. In: Ahrens, U., Diehl, M., Schmehl, R. (eds.) Airborne Wind Energy, Green Energy and Technology, Chap. 8, pp. 141–165. Springer, Berlin Heidelberg (2013). doi: 10.1007/978-3-642-39965-7_8
10. Faggiani, P.: Pumping Kites Wind Farm. M.Sc.Thesis, Delft University of Technology, 2015. http://resolver.tudelft.nl/uuid:66cddbd2-5f50-4fc7-be0b-468853128f37
11. Faggiani, P., Schmehl, R. S., Vlugt, R. van der: Pumping Kites Wind Farm. In: Schmehl, R. (ed.). Book of Abstracts of the International Airborne Wind Energy Conference 2015, pp. 102–103, Delft, The Netherlands, 15–16 June 2015. doi: 10.4233/uuid:7df59b79-2c6b-4e30-bd58-8454f493bb09. Poster available from: http://www.awec2015.com/images/posters/AWEC15_Faggiani-poster.pdf
12. Fechner, U., Schmehl, R.: Model-Based Efficiency Analysis of Wind Power Conversion by a Pumping Kite Power System. In: Ahrens, U., Diehl, M., Schmehl, R. (eds.) Airborne Wind Energy, Green Energy and Technology, Chap. 14, pp. 249–269. Springer, Berlin Heidelberg (2013). doi: 10.1007/978-3-642-39965-7_14
13. Fechner, U., Schmehl, R.: Flight Path Control of Kite Power Systems in a Turbulent Wind Environment. In: Proceedings of the 2016 American Control Conference (ACC), pp. 4083–4088, Boston, MA, USA, 6–8 July 2016. doi: 10.1109/ACC.2016.7525563
14. Goldstein, L.: Density of Individual Airborne Wind Energy Systems in AWES Farms. http://www.awelabs.com/wp-content/uploads/AWES_Farm_Density.pdf (2014). Accessed 19 May 2016
15. Grete, C.: The Economic Potential of Kite Power. Journal of the Society of Aerospace Engineering Students VSV Leonardo da Vinci October, 10–11 (2014). http://resolver.tudelft.nl/uuid:f852545f-2946-4556-9ef8-0b5cdbdaf289
16. Heilmann, J.: Technical and Economic Potential of Airborne Wind Energy. M.Sc.Thesis, Utrecht University, 2012. http://dspace.library.uu.nl/handle/1874/258716
17. Heilmann, J., Houle, C.: Economics of Pumping Kite Generators. In: Ahrens, U., Diehl, M., Schmehl, R. (eds.) Airborne Wind Energy, Green Energy and Technology, Chap. 15, pp. 271–284. Springer, Berlin Heidelberg (2013). doi: 10.1007/978-3-642-39965-7_15
18. Loyd, M. L.: Crosswind kite power. Journal of Energy **4**(3), 106–111 (1980). doi: 10.2514/3.48021
19. Luchsinger, R. H.: Pumping Cycle Kite Power. In: Ahrens, U., Diehl, M., Schmehl, R. (eds.) Airborne Wind Energy, Green Energy and Technology, Chap. 3, pp. 47–64. Springer, Berlin Heidelberg (2013). doi: 10.1007/978-3-642-39965-7_3
20. OECD/NEA/IEA: Projected Costs of Generating Electricity 2010, OECD Publishing, Paris, 2010. 218 pp. doi: 10.1787/9789264084315-en
21. Schmehl, R.: Traction Power Generation with Tethered Wings - A Quasi-Steady Model for the Prediction of the Power Output. In: Schmehl, R. (ed.). Book of Abstracts of the International Airborne Wind Energy Conference 2015, pp. 38–39, Delft, The Netherlands, 15–16 June 2015. doi: 10.4233/uuid:7df59b79-2c6b-4e30-bd58-8454f493bb09. Presentation video recording available from: https://collegerama.tudelft.nl/Mediasite/Play/02a6612b8d004580b08681efd10611351d
22. Schmehl, R., Noom, M., Vlugt, R. van der: Traction Power Generation with Tethered Wings. In: Ahrens, U., Diehl, M., Schmehl, R. (eds.) Airborne Wind Energy, Green Energy and Technology, Chap. 2, pp. 23–45. Springer, Berlin Heidelberg (2013). doi: 10.1007/978-3-642-39965-7_2
23. TKI Wind op Zee: Exploratory Research and LCOE of Airborne Offshore Wind Farm, Project Number TEWZ116048. https://topsectorenergie.nl/tki-wind-op-zee/exploratory-research-and-lcoe-airborne-offshore-wind-farm (2017). Accessed 1 June 2017
24. Vlugt, R. van der, Bley, A., Schmehl, R., Noom, M.: Quasi-Steady Model of a Pumping Kite Power System. Submitted to Renewable Energy (2017). arXiv:1705.04133 [cs.SY]

25. Vlugt, R. van der, Peschel, J., Schmehl, R.: Design and Experimental Characterization of a Pumping Kite Power System. In: Ahrens, U., Diehl, M., Schmehl, R. (eds.) Airborne Wind Energy, Green Energy and Technology, Chap. 23, pp. 403–425. Springer, Berlin Heidelberg (2013). doi: 10.1007/978-3-642-39965-7_23
26. Zaaijer, M.: Great Expectations for Offshore Wind Turbines. Ph.D. Thesis, Delft Univeristy of Technology, 2013. doi: 10.4233/uuid:fd689ba2-3c5f-4e7c-9ccd-55ddbf1679bd